

# Cooperative Adaptive Cruise Platoon Controller Design Considering Switching Control and Stability

Hao Wang, Tiancheng Ruan, Zewen Zuo, Yuxuan Hou, Rui Jiang,

**Abstract**—With the development of Cooperative Adaptive Cruise Control (CACC) technology, CACC Market Penetration Rate (MPR) is expected to increase rapidly, resulting in more CACC platoons. However, the single vehicle control mode makes it difficult to take full advantage of the gain of CACC for capacity. Moreover, the platoon control model with a fixed platoon size is also ineffective since the size of the CACC platoon is arbitrary depending on the dispersion of CACCs and Manual Vehicles (MVs). Therefore, this paper first proposed a novel switching control mode — Cooperative Adaptive Cruise Platoon Control (CACPC)—that takes the CACC platoon as the control object and is adaptive to the platoon size to utilize the CACC technology further. Secondly, a switching control method, Youla-Kučera (YK) parameterization, was adopted to construct a controller class that can stabilize the CACC platoon, thus ensuring stability while the controller switches as the platoon size changes. Then, the tuning function as the switching signal of the controller class constructed by YK parameterization is developed so that CACPC can be adaptive to different platoon sizes. Finally, numerical analyses and simulations were conducted to explore the effectiveness of CACPC on dynamic performance. The CACPC can effectively function and ensure the string stability of the CACC platoon under different platoon sizes. Moreover, with YKparameterization, the CACPC can significantly suppress the endogenous perturbation caused by the controller switching signal due to the change of platoon size, specifically reducing the perturbation amplitude from  $2m/s^2$  to  $0.011m/s^2$ .

**Index Terms**—Cooperative adaptive cruise control; Platoon control; Single final string stability; Switching control.

## I. INTRODUCTION

TO maintain safety, mobility, and environmental sustainability as transportation systems develop rapidly, Connected Autonomous Vehicle (CAV) technology has burgeoned and attracted considerable attention in the past decade. The connectivity and automation of the vehicle have been significantly improved. Vehicle-to-Vehicle (V2V) communication technology enables communication and cooperation between vehicles [1, 2, 3].

The most typical application of V2V communication is Cooperative Adaptive Cruise Control (CACC). A vehicle controlled by this type of system automatically follows the

H. Wang, T. Ruan, Z. Zuo and Y. Hou are with the School of Transportation, Southeast University, Nanjing 211189, P.R. China; Jiangsu Key Laboratory of Urban ITS, Southeast University, Nanjing, 210096, P.R. China; Jiangsu Province Collaborative Innovation Center of Modern Urban Traffic Technologies, Southeast University, Nanjing, 210096, P.R. China(e-mail: haowang@seu.edu.cn;ruantiancheng@seu.edu.cn; 220203312@seu.edu.cn;NOTEVENWRONG@outlook.com).

J. Rui is with Key Laboratory of Transport Industry of Big Data Application Technologies for Comprehensive Transport, Ministry of Transport, Beijing Jiaotong University, Beijing, 100044, China(e-mail: jiangrui@bjtu.edu.cn).

Manuscript received September 21, 2022.(Corresponding author: Hao Wang.)

preceding vehicles. Simulation results and field experiments reveal that, compared with traditional vehicles, cooperatively controlled CAVs can maintain a shorter time headway between vehicles [4]. Therefore, consecutively connected vehicles can form a platoon-based driving mode through Cellular vehicle-to-everything (C-V2X) communication to improve traffic efficiency [5, 6, 7]. In extensive research, theoretical analyses and numerical simulations demonstrate that the CACC system is a more promising and attractive platooning technology in capacity, stability, safety, and pollutant emissions [8, 9].

Despite the advantages mentioned above of the CACC system, it will take a long time for the CACC Market penetration rate (MPR) to grow due to the immaturity of CACC technology, as the CACC MPR is estimated to be only 24.8% in 2045, according to the latest research [10]. Therefore, there are heterogeneous traffic flows consisting of Manual Vehicles (MVs) and CACCs on the road. Since CACCs are separated into several CACC platoons with small platoon sizes by MVs, only a small amount of CACCs can guarantee that communication functions properly. Therefore, CACCs that do not communicate properly will degrade into Adaptive Cruise Controls (ACCs) functionally [11, 12].

The primary goal of the ACC and CACC system is to guarantee local stability, which means perturbations will gradually disappear over time [13, 14]. Moreover, most single-vehicle controllers are also designed to maintain the string stability, i.e., the perturbation propagates through the system and will not be amplified [15, 16, 17]. According to research, string stability depends on the desired time gap adopted by the system, which is inversely proportional to capacity [18, 19]. As the desired time gap gets smaller, string stability becomes harder to maintain [20]. It is easy to ensure that CACCs maintain string stability by setting a proper desired time gap; however, it is challenging for ACCs [21, 22, 23]. ACCs are difficult to maintain string stability unless a large desired time gap is set, which takes the capacity as the cost.

With the above conditions, the traditional single-vehicle control mode is challenged, which ensures the string stability of the CACC platoon by guaranteeing the string stability of each CACC. Therefore, the platoon control mode is increasingly attracting attention, considering the CACC platoon as the control objective instead of a single CACC. The primary goal of the platoon control mode is to coordinate the behaviors (accelerations or decelerations) of all of the following vehicles in the CAV platoon and optimize platoon control based on a specific objective function [24, 25, 26]. Although the effect of the ACC on string stability mainly deteriorates, the gain of the CACC can effectively suppress this deterioration. Specifically,

by setting the desired time gaps of the CACC and ACC appropriately, the string stability of the platoon formed by the ACC and CACC is guaranteed, even if the ACC does not. Moreover, thanks to the benefit of CACC on string stability, the desired time gap can be set lower while maintaining string stability as the CAV platoon size increases [27]. Wang et al. [24] develop a robust cooperative control strategy to ensure the safe and efficient maneuvering of a CAV platoon in the worst-case situation due to the uncertainties in the vehicle dynamics. Shen et al. [25] propose a fully distributed optimization-based platoon-centred CAV platooning control via model predict control with a broad prediction horizon. Numerical tests demonstrate the effectiveness of the proposed fully distributed schemes and CAV platooning control on transient traffic performance and string stability. Xu et al. [26] propose an energy-oriented robust platoon control strategy based on the  $H_\infty$  method, which enables efficient driving of each vehicle while ensuring the platoon string stability.

While the aforementioned platoon control strategies can coordinate the car-following behaviors of CAVs in a platoon effectively, most of the platoon control strategies are stationary, i.e., the control strategy performs optimal control for a specific optimal objective after the CAV platoon is formed. Such platoon control strategies can effectively improve the performance of the CAV platoon by improving the control objective. However, the design of platoon control strategy without paying attention to different CAV platoon sizes leads to its limitation and does not function properly when the platoon size changes. Furthermore, limited by the slow growth of CACC MPRs, the platoon sizes of several CACC platoons separated by MVs are arbitrary, depending on the dispersion of CACCs and MVs on the road [28]. Therefore, the CACC platoon control mode with a fixed platoon size does not function effectively. To this end, an adaptive CACC platoon control strategy according to the platoon size is required to exploit the gain of CACC for traffic flow effectively.

In addition, the platoon control strategies in existing research only focus on optimal control after the formation of the CAV platoon and ignore the platoon forming and splitting process. The process of controller switching during platoon forming and splitting can lead to significant autogenous perturbation, which is one of the factors of system insecurity [29]. Even if the controllers are stable before and after switching, they are not always stable during the switching process. Therefore, a switching control strategy that can guarantee the stability of the CACC platoon during controller switching needs to be developed to avoid the insecurity caused by platoon forming and splitting.

In order to leverage the benefit of CACCs, this paper proposed a new decentralized switching control mode named Cooperative Adaptive Cruise Platoon Control (CACPC) that takes the CACC platoon as the control objective and adaptively switches as the platoon size changes. Firstly, we determined the minimum combination of desired time gaps before and after the controller switching based on string stability analyses to maximize the capacity. Secondly, the conventional control structures of the ACC and CACC are modified to an equivalent Youla-Kučera (YK) control structure to construct a controller

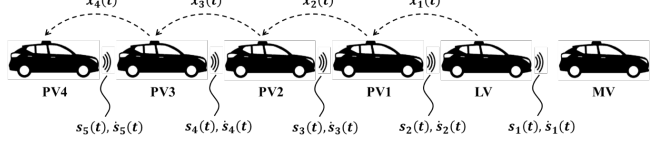


Fig. 1: Schematic of CACC platoon.

class that can stabilize the CACC platoon based on YK parameterization. The third, the tuning function as a switching signal, was developed to ensure the applicability under different platoon sizes. Finally, the effectiveness of CACPC on dynamic performance was explored.

The rest of this paper is organized as follows. Section. II introduces the CACC system setup, control objectives, and control structure studied in this paper. Section. III proposes the primary methodologies, including string stability analyses and YK parameterization. The detailed controller design process of YK parameterization is presented in Section. IV. Section. V validates the theoretical results and explores the impact of CACPC. The conclusion is summarized in Section. VI.

## II. PROBLEM FORMULATION

This section mainly introduces the background knowledge of the problems studied in this paper from three perspectives: CACC system setup, control objectives, and control structure.

### A. CACC System Setup

Fig. 1 shows a schematic of the CACC platoon, where  $s_i(t), \dot{s}_i(t)$  indicate the relative gap and relative velocity that CACC obtained through the onboard sensor, and  $\ddot{x}_{i-1}(t)$  is the acceleration of the predecessor vehicle obtained through V2V communication.

The CACC design is based on a standard ACC system with a communication module. A CACC platoon can be divided into a Lead Vehicle (LV) and  $S - 1$  Platoon vehicles (PV)s based on the communication ability of the predecessor vehicle, where  $S$  denotes the maximum size of a CACC platoon. Notice that the CACC platoon cannot be infinitely long due to the limitation of the unreliable communication environment. Therefore, we assume the maximum platoon size is the platoon size that can keep communication functioning well. The LVs degrade to ACCs functionally because the predecessor vehicle is an ACC or MV, which cannot communicate, while the communication module of PVs is functioning [30, 31].

Considering the feasibility of implementation, the controller used in this paper is a decentralized controller instead of a centralized one. The specific information flow topology (IFT) is predecessor following (PF) which means CACCs only communicate with the nearest predecessor to gain further information in advance. As for spacing policy, Constant Time Gap (CTG), including a constant and a velocity-dependent part, is applied due to its widespread use.

### B. String stability

We have considered the nuances in different definitions of string stability in the literature. In this paper, the single final

string stability is adopted [32]. Namely, the perturbation only affects the lead vehicle and will not be amplified relative to the response of the last vehicle [33, 34, 35, 28, 15], i.e., between vehicle LV to vehicle PV4 (see Fig. 1). As for specific spacing policy, the error  $e_i(t)$  between the desired and actual inter-vehicle gap is frequently considered in CTG to prevent collisions.

In this paper, the single final string stability of the CACC platoon is studied as a whole instead of analyzing each CACC in the platoon. To facilitate the analysis and focus on the amplification of perturbation, a frequency-domain approach is adopted to obtain a necessary and sufficient condition for the single final string stability of the CACC platoon, which will provide support for designing CACPC.

### C. Control Structure

The CACC design is based on a standard ACC system and applies the most commonly used CTG policy. In this subsection, the control structures of the ACC and CACC system are discussed, respectively, to study the subsequent design of CACPC.

It is assumed that each CACC is equipped with i) an on-board radar responsible for collision detection via measuring the gap distance between any two consecutive vehicles, ii) a built-in GPS sensor for measuring the vehicular longitudinal position information, iii) a wireless on-board unit for communicating information of interest with its proximal vehicles via the C-V2X communication, iv) an upper-level controller for calculating the desired longitudinal acceleration based on the parameters obtained, and v) a lower-level controller for determining the throttle and brake actuator inputs so as to track the desired acceleration. Such an assumption is reasonable as the sensing, communication, and actuation units requested above are available in modern CAVs, and thus do not require specific changes in the existing vehicle configuration. Note that the on-board radar only functions when the CACC degrades to the ACC if communication is unavailable or malfunctioning since more accurate information can be obtained faster via communication.

Moreover, we remark that this paper only focuses on homogeneous CACCs where CACCs have the same control structure and controller parameters.

#### 1) ACC Control Structure:

The primary control object of the ACC system is to maintain the desired gap from the preceding vehicle  $s_{d,i}(t) = r_i + L_i + h_i \dot{x}_i(t)$ , including a velocity-dependent part and a constant part, where  $L_i$  represents the vehicle length,  $r_i$  is the standstill distance,  $x_i$  denotes the longitudinal position of vehicle  $i$  and  $h_i$  represents the desired time gap of vehicle  $i$ . Using the onboard sensor, the relative gap  $s_i(t) = x_{i-1}(t) - x_i(t)$  and relative velocity  $\dot{s}_i(t)$  are measured. In a standard ACC system, the feedback controller controls the error  $e_i(t) = s_i(t) - s_{d,i}(t)$  between the desire gap and relative gap.

The ACC control structure is schematically depicted in Fig. 2 (a).

As shown in Fig. 2 (a), the ACC control structure is represented as a system construction drawing with vehicle

position as input and output. The model  $K_i(s)$  is the ACC feedback gain, which can be given as:

$$K_i(s) = k_p + k_d s, \quad (1)$$

where  $k_p$  is error gain and  $k_d$  is error speed gain, the specific parameter setting is based on previous research [36, 37].

The model  $G_i(s)$  denotes a lower level controller representing longitudinal vehicle dynamics, where the input  $u_i(t)$  of  $G_i(s)$  is the desired acceleration derived from  $K_i(s)$  and the output  $x_i(t)$  is the output position based on the control loop to track desired acceleration through actuation of the throttle and brake system. The linear transfer function of  $G_i(s)$  can be represented by [17]:

$$G_i(s) = \frac{k_G}{s^2(\tau_i s + 1)} e^{-\phi_i s}, \quad (2)$$

where  $\tau_i^{-1} = \omega_{bw,l,i}$  is the closed-loop bandwidth,  $k_G$  is the model gain and  $\phi_i$  is the time delay of vehicle actuator and intra-vehicle communication, the specific parameter setting is shown in Table I based on the field experiments in Appendix A.

Model  $H_i(s)$  is the ACC feedback gain, which can be given as:

$$H_i(s) = 1 + h_i s, \quad (3)$$

where  $h_i$  is the desired time gap of vehicle  $i$ .

The closed-loop transfer function of the ACC system in the frequency domain is as follows:

$$\mathcal{J}_{i,ACC}(s) = \frac{X_i(s)}{X_{i-1}(s)} = \frac{G_i(s)K_i(s)}{1 + H_i(s)G_i(s)K_i(s)}, \quad (4)$$

where  $X_i(s)$  is the Laplace transform of  $x_i(t)$ .

#### 2) CACC Control Structure:

As discussed above, the CACC controller is equipped with a communication module that extends the standard ACC feedback controller. The specific control structure is schematically depicted in Fig. 2 (b).

For simplicity, the definitions of model  $H_i(s)$ ,  $G_i(s)$ , and  $K_i(s)$  in the system construction drawing are omitted because they are the same as those in Section II-C1. The acceleration  $\ddot{x}_{i-1}(t)$  of the predecessor vehicle obtained through V2V communication is used as a feedforward control signal through the feedforward filter  $F_i(s)$  and the communication delay model  $D_i(s)$ .

The model  $D_i(s)$  is directly related to the constant communication delay  $\theta_i$ , which can be expressed as:

$$D_i(s) = e^{-\theta_i s}, \quad (5)$$

where  $\theta_i$  represents the constant communication delay. The specific parameter setting is according to previous research [20, 38].

The model  $F_i(s)$  is the communication feedforward filter which can be given as:

$$F_i(s) = (H_i(s)G_i(s))^{-1}. \quad (6)$$

The closed-loop transfer function of the CACC system in

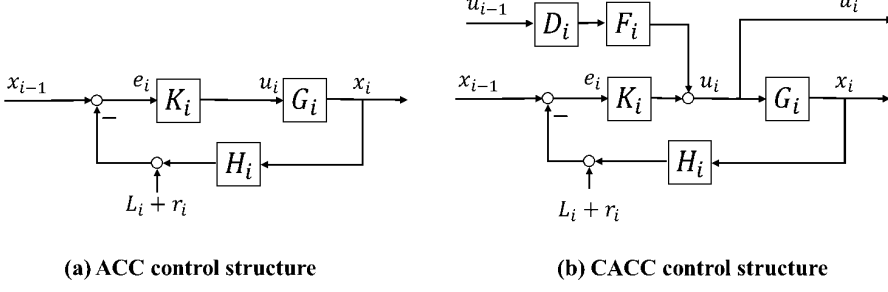


Fig. 2: Control structure of ACC and CACC: (a) ACC; (b) CACC.

the frequency domain is as follows:

$$\mathcal{J}_{i,CACC}(s) = \frac{X_i(s)}{X_{i-1}(s)} = \frac{(K_i(s) + D_i(s)F_i(s))G_i(s)}{1 + H_i(s)G_i(s)K_i(s)}. \quad (7)$$

### 3) CACPC structure:

As the control system for the controller design in this paper, the CACC platoon is designated as the primary control unit for string stability analyses. We can couple the control structure of ACC and CACC by merging the inner and outer signals, thus establishing the structure of CACPC. The specific structure of the CACPC is schematically depicted in Fig. 3.

For simplicity, the definitions of model  $H_i(s)$ ,  $G_i(s)$ ,  $K_i(s)$  and  $D_i(s)$  in system construction drawing are omitted because they are the same as those in Section. II-C1 and II-C2.

The closed-loop transfer function of CACPC system in the frequency domain is as follows:

$$\begin{aligned} \mathcal{J}_{\text{platoon}}(s) &= \frac{X_n(s)}{X_0(s)} = \frac{X_n(s)}{X_{n-1}(s)} \frac{X_{n-1}(s)}{X_{n-2}(s)} \dots \frac{X_1(s)}{X_0(s)} \\ &= \mathcal{J}_{1,ACC}(s) \prod_{i=2}^n \mathcal{J}_{i,CACC}(s), \end{aligned} \quad (8)$$

where  $n$  denotes the platoon size.

## III. METHODOLOGY

In this section, the primary methodology applied in this paper is introduced, including the transfer function method for string stability analyses and the YK parameterization for controller switching.

### A. String stability analysis

Laplace transform is a classic method to explore string stability in a direct and precise manner. Moreover, it has been adopted in extensive research [39, 40, 41]. Therefore, single final string stability analyses of this paper are conducted based on the Laplace transform. The relationship of the perturbation propagating through the CACC platoon in the frequency domain is:

$$\mathcal{J}_{\text{platoon}}(s) = \frac{X_n(s)}{X_0(s)}. \quad (9)$$

According to the definition of string stability, a sufficient and necessary conservative condition for string stability can be derived according to the  $\mathcal{L}_\infty$  norm:

$$\|x_n(t)\|_{\mathcal{L}_\infty} \leq \|x_0(t)\|_{\mathcal{L}_\infty} \quad (10)$$

where  $x_n(t)$  and  $x_0(t)$  are the inverse Laplace transformation of  $X_n(s)$  and  $X_0(s)$ , respectively;  $\|\cdot\|_{\mathcal{L}_\infty}$  is the  $\mathcal{L}_\infty$  norm, which deals with the peak of perturbations.

Moreover, according to the relationship  $\|g\|_1 = \sup_{x \in L_\infty} \frac{\|y\|_{\mathcal{L}_\infty}}{\|x\|_{\mathcal{L}_\infty}}$  Equation(10) can be replaced as:

$$\|j(t)\|_1 \leq 1 \quad (11)$$

where  $j(t)$  denotes the impulse response of  $\mathcal{J}_{\text{platoon}}(s)$ .

Furthermore, the Equation(11) can be replaced by the following two conditions [42]:

$$\|\mathcal{J}_{\text{platoon}}(s)\|_\infty \leq 1 \quad \& \quad j(t) > 0 \quad (12)$$

We remark that we adopt  $\mathcal{L}_\infty$  norms of the string stability instead of  $\mathcal{L}_2$  norms. Although  $\mathcal{L}_2$  norms can provide more explicit derivation, it only deals with the energy dissipation in the upstream direction and not the peak of perturbations [43]. In addition, the single final string stability is adopted in this paper for string stability analyses since it can deal with the relationship between peaks of perturbation before and after it spreads over the platoon. So that the string stability indicates the perturbation is not amplified by the CACC platoon [44].

### B. Controller switching method: Youla-Kucera parametrization

Maintaining string stability of the CACC platoon is one of the primary control objectives. However, this control objective is difficult for the CACC platoon with variable platoon size because it implies a compromise between string stability and capacity. Therefore an adaptive controller design approach for platoon size is needed to maintain string stability while maximizing capacity. Besides, adapting to the platoon size leads to another problem: the controller switching when the platoon size changes. Direct controller switching is a transient process that is chaotic, meaning that the intermediate states do not necessarily remain stable even if the controllers are stable before and after switching. Moreover, controller switching will inevitably trigger endogenous perturbations, which will cause safety hazards in the traffic flow. Therefore, a parameterization method for smooth switching between different controllers is needed to ensure the feasibility of the above CACC controllers design.

Youla-Kucera (YK) parameterization is a method to stabilize the class of a given plant that contains all stabilizing controllers [45, 46]. One of the advantages of this method is that

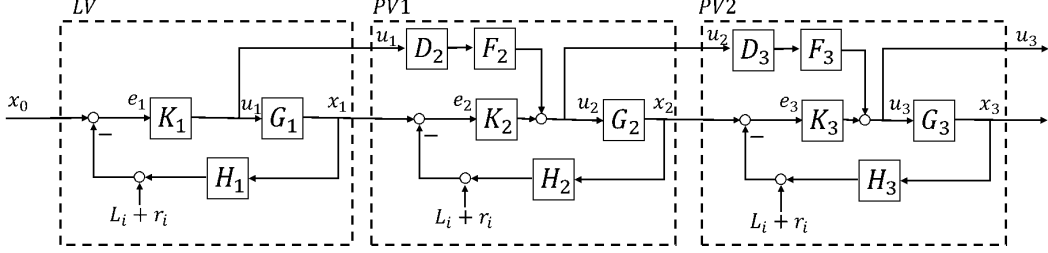


Fig. 3: CACPC structure.

the performance transfer function is tuned with a particular parameter, which means that the stability of unstable open-loop controllers can be maintained while switching between controllers. It is worth noting that the switching controller designed using YK parametrization is a controller class consisting of a set of stabilizing controllers based on a tuning function and a parameter. Therefore, the YK parametrization can transform the controller switch into a change in the tuning function and thus avoid strong endogenous perturbations due to direct changes in the controller.

The basis of YK parametrization is described in detail below, which includes doubly coprime factorization and YK parameterization of all stabilizing controllers.

Basic notations are introduced below.  $\mathbb{R}H_\infty$  is the real stable transfer function space;  $G$  and  $K_i$  maintain the same definitions as in Section. III.

### 1) Fundamentals on YK parametrization:

Before applying YK parametrization, the internal dynamics of the vehicles  $G$  need to be presented as state-space representation for subsequent analyses:

$$\begin{aligned}\dot{m}(t) &= Am(t) + Bu(t), \\ x(t) &= Cm(t) + Du(t)\end{aligned}, \quad G(s) = \begin{bmatrix} A & B \\ C & D \end{bmatrix}, \quad (13)$$

where  $t$  indicates time,  $m(t)$  is the state vector,  $\dot{m}(t)$  is the evolution of the state vector over time,  $x(t)$  is the output vector, and  $u(t)$  is the control vector.  $A$ ,  $B$ ,  $C$ , and  $D$  are the constant coefficients matrices of state-space matrices of  $G$ .

Then any appropriate controller  $K_i$  could stabilize this system, which is represented as:

$$\begin{aligned}\dot{n}(t) &= A_i^c n(t) + B_i^c e(t), \\ u(t) &= C_i^c n(t) + D_i^c e(t)\end{aligned}, \quad K_i(s) = \begin{bmatrix} A_i^c & B_i^c \\ C_i^c & D_i^c \end{bmatrix}, \quad (14)$$

where  $n(t)$  is the state vector, and  $A_i^c, B_i^c, C_i^c$  and  $D_i^c$  are the constant coefficients matrices of state-space matrices of  $K_i$ . Note that we choose  $K_0$  represents the initial controller, and  $K_1$  represents the controller after a complete switch.

### 2) Doubly coprime factorization:

Double coprime factorization is one of the keys to YK parameterization. Coprime factors are obtained by coprime factorization of the plant and controllers. Then the stabilizing controller class corresponding to the plant  $G$  can be derived through interpolation. In this process, factorization means the plant and controllers are represented as the products of two transfer functions. Coprimeness refers to the absence of

common zeros in the right half-plane, and double coprimeness excludes unstable pole/zero cancellations and refers to the idea of being right and left coprime.

The coprime factors of  $G$  and  $K_i$  can be expressed as:

$$G = NM^{-1} = \tilde{M}^{-1}\tilde{N}, \quad K_i = U_i V_i^{-1} = \tilde{V}_i^{-1}\tilde{U}_i, \quad (15)$$

where coprime factors  $N, M, \tilde{M}, \tilde{N}, U_i, V_i, \tilde{U}_i, \tilde{V}_i \in \mathbb{R}H_\infty$  satisfy double Bezout's identity [47]:

$$\begin{bmatrix} \tilde{V}_i & -\tilde{U}_i \\ -\tilde{N} & \tilde{M} \end{bmatrix} \begin{bmatrix} M & U_i \\ N & V_i \end{bmatrix} = \begin{bmatrix} M & U_i \\ N & V_i \end{bmatrix} \begin{bmatrix} \tilde{V}_i & -\tilde{U}_i \\ -\tilde{N} & \tilde{M} \end{bmatrix} = \begin{bmatrix} I & 0 \\ 0 & I \end{bmatrix}. \quad (16)$$

Using the relationship of state-space representation and transfer function  $G(s) = C(sI - A)^{-1}B$  and  $K_i(s) = C_i^c(sI - A_i^c)^{-1}B_i^c + D_i^c$ , coprime factors can be expressed by:

$$\begin{bmatrix} M & U_i \\ N & V_i \end{bmatrix} = \left[ \begin{array}{cc|cc} A + BF & 0 & -B & 0 \\ 0 & A_i^c + B_i^c F_i^c & 0 & B_i^c \\ -F & C_i^c + D_i^c F_i^c & I & D_i^c \\ -C & F_i^c & 0 & I \end{array} \right], \quad (17)$$

$$\begin{bmatrix} \tilde{V}_i & -\tilde{U}_i \\ -\tilde{N} & \tilde{M} \end{bmatrix} = \left[ \begin{array}{cc|cc} A + BD_i^c C & BC_i^c & -B & BD_i^c \\ B_i^c C & A_i^c & 0 & B_i^c \\ F_i - D_i^c C & -C_i^c & I & -D_i^c \\ C & -F_i^c & 0 & I \end{array} \right], \quad (18)$$

where  $F$  and  $F_i^c$  should be chosen such that  $A + BF, A_i^c + B_i^c F_i^c \in \mathbb{R}H_\infty$ . Straight lines indicate the elements of the matrix that belong to each factor respectively. The proof of the Equation (17-18) is detailed in Appendix B.

Note that only the controller switches from  $K_0$  to  $K_1$  during the process of controller switching, and the internal dynamics of the vehicles  $G$  remain unchanged. Therefore, the coprime factors of  $G$  ( $M$  and  $N$ ) remain unchanged while the coprime factors of  $K_0$  ( $U_0, V_0$ ) and  $K_1$  ( $U_1, V_1$ ) are switching.

### 3) YK parameterization of all stabilizing controllers:

The most critical step of YK parameterization is to establish a controller class containing all controllers that can stabilize a given plant  $G$  through a parameter  $Q$  based on coprime factors of the plant  $G$  and controllers  $K_i$  before and after switching. Through controller interpolation, the expressions of  $K(Q)$  and  $Q$  are derived as:

$$\begin{aligned}K(Q) &= (U_0 + M\gamma Q)(V_0 + N\gamma Q)^{-1} \\ &= (\tilde{V}_0 + \gamma Q\tilde{N})^{-1}(\tilde{U}_0 + \gamma Q\tilde{M}), \quad Q \in \mathbb{R}H_\infty^{p,xm},\end{aligned} \quad (19)$$

$$Q = \tilde{U}_1 - \tilde{V}_1 \tilde{V}_0^{-1} \tilde{U}_0, \quad (20)$$

where  $\gamma \in [0, 1]$  is a scalar factor playing a pivotal role as a switching signal in controller interpolation, indicating the level of interconnection of the two controllers [48]. When  $\gamma = 0$ , the controller is completely taken over by  $K_0$ , while  $K_1$  is fully controlled when  $\gamma = 1$ .

**Proof:** First, check the matrix of the closed-loop feedback control system.

$$\begin{aligned} & \left[ \begin{array}{cc} I & -K(Q) \\ -G & I \end{array} \right]^{-1} \\ &= \left[ \begin{array}{cc} I & -(\tilde{V}_0 + \gamma Q \tilde{N})^{-1} (\tilde{U}_0 + \gamma Q \tilde{M}) \\ -\tilde{M}^{-1} \tilde{N} & I \end{array} \right]^{-1} \\ &= \left\{ \begin{bmatrix} (\tilde{V}_0 + \gamma Q \tilde{N})^{-1} & 0 \\ 0 & \tilde{M}^{-1} \end{bmatrix} \begin{bmatrix} \tilde{V}_0 + \gamma Q \tilde{N} & -(\tilde{U}_0 + \gamma Q \tilde{M}) \\ -\tilde{N} & \tilde{M} \end{bmatrix} \right\}^{-1} \\ &= \begin{bmatrix} M & U_0 + M\gamma Q \\ N & V_0 + N\gamma Q \end{bmatrix} \begin{bmatrix} \tilde{V}_0 + \gamma Q \tilde{N} & 0 \\ 0 & \tilde{M} \end{bmatrix} \\ &= \left\{ \begin{bmatrix} M & U \\ N & V \end{bmatrix} + \begin{bmatrix} 0 & \gamma M Q \\ 0 & \gamma N Q \end{bmatrix} \right\} \left\{ \begin{bmatrix} \tilde{V} & 0 \\ 0 & \tilde{M} \end{bmatrix} + \begin{bmatrix} \gamma Q \tilde{N} & 0 \\ 0 & 0 \end{bmatrix} \right\}^{-1} \\ &= \begin{bmatrix} M & U \\ N & V \end{bmatrix} \begin{bmatrix} \tilde{V} & 0 \\ 0 & \tilde{M} \end{bmatrix} + \begin{bmatrix} \gamma M Q \tilde{N} & 0 \\ \gamma N Q \tilde{N} & 0 \end{bmatrix} + \begin{bmatrix} 0 & \gamma M Q \tilde{M} \\ 0 & \gamma N Q \tilde{M} \end{bmatrix} \\ &= \begin{bmatrix} \tilde{V} & -\tilde{U} \\ -\tilde{N} & \tilde{M} \end{bmatrix}^{-1} \begin{bmatrix} \tilde{V}^{-1} & 0 \\ 0 & \tilde{M}^{-1} \end{bmatrix}^{-1} + \begin{bmatrix} \gamma M Q \tilde{N} & \gamma M Q \tilde{M} \\ \gamma N Q \tilde{N} & \gamma N Q \tilde{M} \end{bmatrix} \\ &= \begin{bmatrix} M & U \\ N & V \end{bmatrix} \begin{bmatrix} \tilde{V} & 0 \\ 0 & \tilde{M} \end{bmatrix} + \begin{bmatrix} M \\ N \end{bmatrix} \gamma Q \begin{bmatrix} \tilde{N} & \tilde{M} \end{bmatrix} \\ &= \begin{bmatrix} I & -K \\ -G & I \end{bmatrix}^{-1} + \begin{bmatrix} M \\ N \end{bmatrix} \gamma Q \begin{bmatrix} \tilde{N} & \tilde{M} \end{bmatrix} \in \mathbb{R}H_\infty^{p,xm}. \end{aligned} \quad (21)$$

From Equation (21), it is clearly that any controller  $K(Q)$  parameterized by  $Q \in \mathbb{R}H_\infty^{p,xm}$  stabilizes the plant  $G$  according to the Corollary 4.2 in references [49, 50].

In addition, the factors affecting the functioning controllers during switching contain only the tuning function  $\gamma$  and coprime factors of the plant  $G$  and controllers  $K_i$ . Since the plant  $G$  and controllers  $K_i$  do not change in the switching process, their coprime factors do not change either. Therefore, during controllers switching, the functioning controllers included in the controller family  $K(Q)$  are only affected by the tuning function  $\gamma$ . Moreover, the closed-loop poles of the system during the switching process are the combination of  $[G, K_0]$  and  $[G, K_1]$ , which can maintain the stability of the system under any combination of  $Q$  and  $\gamma$ , thus ensuring the stable switch of the controllers independent of  $\gamma$  [48].

#### IV. YK PARAMETERIZATION

In this section, the detailed controller design process is carried out using the methodology proposed in Section. III. Specifically, the CACC platoon controller design process based on YK parameterization includes:

- 1) Selecting the desired time gap before and after the controller switching based on string stability analyses;
- 2) Modifying the control structure proposed in Section. II-C to YK control structure and calculating the coprime

TABLE I: Parameters chosen for ACC and CACC controller.

| Parameter | $k_p$                | $k_d$                | $\tau_i$     | $k_G$  | $\phi_i$ | $\theta_i$ |
|-----------|----------------------|----------------------|--------------|--------|----------|------------|
| Value     | 0.45 s <sup>-2</sup> | 0.25 s <sup>-1</sup> | 0.7862 s/rad | 0.9403 | 0.2 s.   | 0.3 s      |

factors of the controllers before and after switching and YK parameters  $Q$ ;

- 3) Determining the tuning function  $\gamma$  for different platoon sizes according to the string stability analyses results and YK control structure in Section. IV-B.

In addition, to facilitate subsequent calculations and experiments, the above-defined controller coefficients selected in this paper are as follows, which are set based on existing research [20, 36, 37] and field experiments employed detailed in Appendix A. The specific parameter setting is shown in Table. I. Moreover, the maximum platoon size  $S$  of the CACC platoon is set to 5 in the paper, which is absolutely feasible and effective for communication latency and packet loss rates from the perspective of the communication technology.

#### A. Analyses of string stability

When the CACC platoon is formed, taking the CACC platoon as the control object can maintain a smaller desired time gap without losing string stability. Note that the CACC platoon contains the lead ACC (which is a CACC but degraded to an ACC functionally) and several CACCs, the desired time gaps of the ACC and CACCs are different. Therefore, we need to investigate not only the minimum desired time gaps of the ACC and CACCs but also the minimum desired time gap combination for the CACC platoon. The corresponding theoretical analyses regarding string stability are carried out using the method proposed in Section. III-A.

As for the desired time gap  $h_i = h_{i,min}$ , margin string stability criterion (12) is met, and string stability can be guaranteed when  $h_i \geq h_{i,min}$  [51]. However, due to the complexity of the CACPC structure, the calculation of the minimum desired time gap  $h_{i,min}$  is too complicated and cannot give an algebraic equation of  $h_{acc}$  and  $h_{cacc}$ , so the derivation is not discussed here. A numerical approximation approach is adopted to explore the combination of  $h_{min,acc}$  and  $h_{min,cacc}$  as margin string stable according to Equation (12). Moreover, since the perturbation faced in real traffic conditions is considered to be of infinite wavelength [52, 53], we only focus on the magnitude of the transfer function under low frequency ( $10^{-5} - 10^0$  Hz) [54]. Fig. 4 shows that  $h_{min,cacc}$  changes with  $h_{min,acc}$  over different frequencies where the heatmap shows the margin stable combination of  $h_{min,cacc}$  and  $h_{min,acc}$  under different perturbation frequency and the colored contour lines represent the stability demarcation lines of the combination of  $h_{min,cacc}$  and  $h_{min,acc}$  under perturbation frequency.

It can be clearly found in Fig. 4 that CACC can maintain a smaller desired time gap with platoon size increasing. Moreover,  $h_{min,cacc}$  can significantly decrease with  $h_{min,acc}$  increasing, which means the feasibility of eliminating the redundancy within the CACC platoon through the appropriate deployment of the desired time gap. In addition, string stability

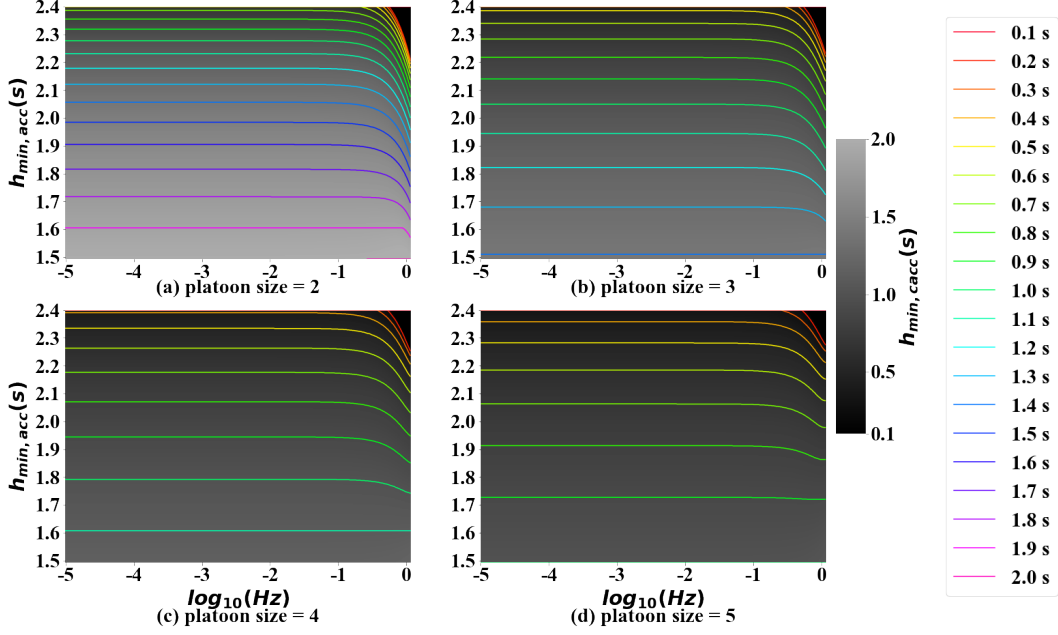


Fig. 4: Contour plot of perturbation frequency versus  $h_{min,acc}$ , indicating the corresponding minimal value for  $h_{min,cacc}$ .

can be significantly improved as the frequency of perturbation approaches  $10^0$  Hz, which is represented as the arc under  $10^{-0.5} - 10^0$  Hz in Fig. 4. When we focus on the region of  $10^{-5} - 10^{-0.5}$  Hz, an interesting phenomenon is discovered that  $h_{min,cacc}$  stays the same as the frequency increases, which means the combination of  $h_{min,cacc}$  and  $h_{min,acc}$  to guarantee the string stability is determined for a specific platoon size.

Based on the conclusions obtained above, in order to maximize the capacity while ensuring string stability and safety, we choose  $h_{1,acc} = 2s$  and  $h_{1,cacc} = 0.4s$  for the case of  $S = 5$  which indicates the controller after switching while the desired time gap settings of ACC and CACC for the case of  $S = 2$  are  $h_{0,acc} = 2.108s$  and  $h_{0,cacc} = 0.747s$  adopted by the controller before switching in this paper.

#### B. Analyses of controller switching

Based on the combination of the minimum desired time gap obtained in Section. IV-A, the controller can be determined. Then the control structures proposed in Section. II-C need to be modified to the equivalent YK control structures. In addition, the coprime factors of the controllers and the YK parameters  $Q$  can be derived.

##### 1) Modify ACC controller:

For the LV in a CACC platoon, since it cannot communicate with the predecessor vehicle, it loses the information gained from the communication module, so its control system is represented by standard ACC, as shown in Fig. 2 (a).

To incorporate the desired time gap into the controller, the ACC controller in Fig. 2 (a) is reconstructed so that the ACC controller can perform stable interpolation for the different desired time gaps  $h_i$ . Moreover, the corresponding equivalent

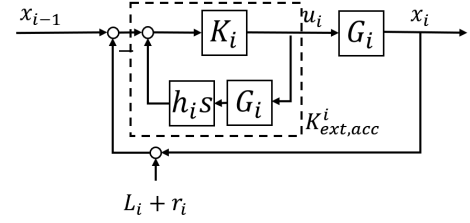


Fig. 5: Equivalent ACC control structure.

ACC control structure is shown in Fig. 5. The transfer function of the extended controller is as follows:

$$K_{ext,acc}^i(s) = \frac{K_i}{1 + h_i G_i K_i s}. \quad (22)$$

##### 2) YK parametrization for ACC controller:

Based on the mathematical basis introduced in Section. III-B, the control structure applied to controller switching needs to be modified accordingly by introducing a dual coprime factor. The control structure for switching based on left coprime factors is shown in Fig. 6:

For stable switching purposes, coprime factors need to meet double Bezout's identity as shown in Equation (16) based on the state-space matrix of transfer functions of  $K_{0,acc}$ ,  $K_{1,acc}$ . In addition, the minimum desired time gap of the controllers before and after switching determined in Section. IV-A is adopted for determining the specific controller. Then the specific transfer function equations for the coprime factors of

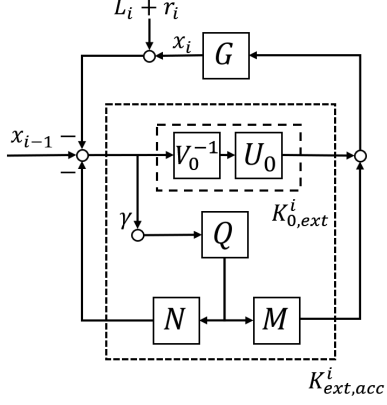


Fig. 6: YK control structure for ACC controllers switching.

$K_{0,acc}$  and  $K_{1,acc}$  are as follows:

$$\begin{aligned} U_0 &= \frac{-s(s+1.272)(s+1.8)}{(s+4.42)(s^2+1.836s+1.027)}, \\ V_0 &= \frac{-4(s^2+1.902s+1.135)}{(s+4.42)(s^2+1.836s+1.027)}, \\ U_1 &= \frac{-s(s+1.272)(s+1.8)}{(s+4.42)(s^2+1.808s+0.9741)}, \\ V_1 &= \frac{-4(s^2+1.87s+1.076)}{(s+4.42)(s^2+1.808s+0.9741)}. \end{aligned} \quad (23)$$

As for the YK parameter  $Q_{acc}$ , substitute coprime factors into Equation(20):

$$Q_{acc} = \frac{-0.1005(s+1.892)(s+4.38)(s+4.42)}{(s^2+1.82s+0.9968)(s^2+1.969s+1.238)} \cdot \frac{(s+4.42)^3(s^2+1.808s+0.9741)(s^2+1.836s+1.027)^2}{(s+4.42)^3(s^2+1.808s+0.9741)(s^2+1.836s+1.027)^2}. \quad (24)$$

### 3) Modify CACC controller:

Similar to the method adopted in Section. IV-B1, the system construction drawing of the CACC controller is in Fig. 3, which is reconstructed to incorporate the desired time gap  $h_i$  into the controller. Furthermore, the corresponding equivalent CACC control structure is shown in Fig. 7. The transfer function of the extended controller is as follows:

$$K_{ext,cacc}^i(s) = \frac{K_i}{1 + h_i G_i K_i s}. \quad (25)$$

### 4) YK parametrization for CACC controller:

Similar to Section. IV-B2, the control structure applied to controller switching needs to be modified accordingly by introducing a dual coprime factor based on the mathematical basis presented in Section. III-B. The control structure for switching based on left coprime factors is shown in Fig. 8:

Based on Equation (17-18), coprime factors which meet double Bezout's identity, as shown in Equation (16), can be obtained easily. The minimum desired time gap of the controllers before and after switching determined in Section. IV-A

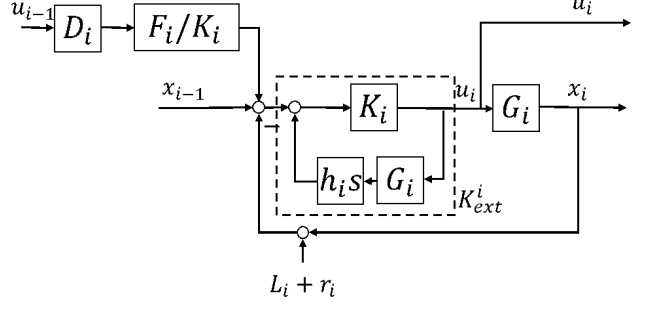


Fig. 7: Equivalent CACC control structure.

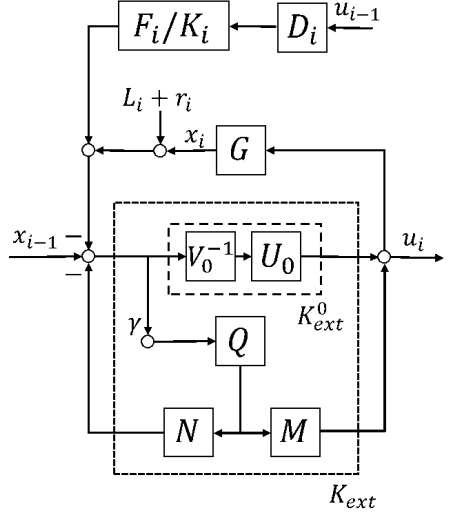


Fig. 8: YK control structure for CACC controllers switching.

is adopted. Then the specific transfer function equations for the coprime factors of  $K_{0,cacc}$  and  $K_{1,cacc}$  are as follows:

$$\begin{aligned} U_3 &= \frac{-s(s+1.272)(s+1.8)}{(s+4.406)(s+1.159)(s+0.3148)}, \\ V_3 &= \frac{-4(s+1.144)(s+0.3515)}{(s+4.406)(s+1.159)(s+0.3148)}, \\ U_4 &= \frac{-s(s+1.272)(s+1.8)}{(s+4.397)(s+1.226)(s+0.1438)}, \\ V_4 &= \frac{-4(s+1.221)(s+0.1587)}{(s+4.397)(s+1.226)(s+0.1438)}. \end{aligned} \quad (26)$$

As for the YK parameter  $Q_{cacc}$ , substitute coprime factors into Equation(20):

$$Q_{cacc} = \frac{-0.4451(s+4.402)(s+3.51)(s+1.918)(s+1.8)}{(s+1.274)(s+1.219)(s+1.414)(s+0.3596)(s+0.1572)} \cdot \frac{(s+4.397)(s+1.8)(s+1.272)(s+1.226)(s+0.1438)}{(s+4.406)^2(s+0.3148)^2(s^2+2.319s+1.344)}. \quad (27)$$

### C. Tuning function $\gamma$ for CACC platoon

The theoretical results of Section. IV-A point out that different CACC platoon sizes have different combinations of  $h_{min,acc}$  and  $h_{min,cacc}$  as string stability margin. In order to

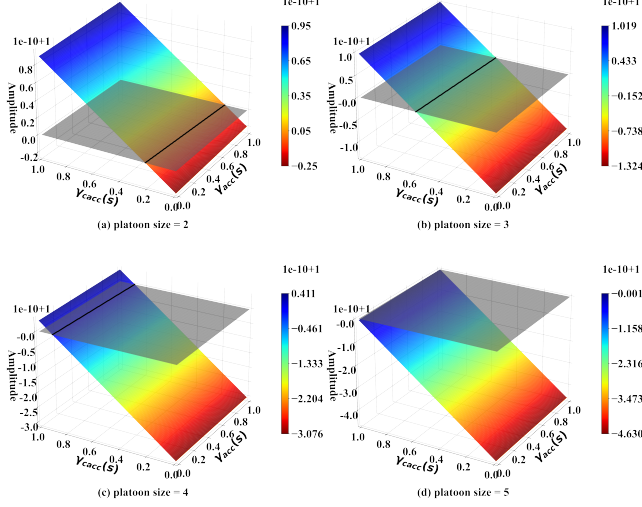


Fig. 9: String stability's surface depending on YK  $\gamma_{acc}$  and  $\gamma_{cacc}$ .

maximize the traffic capacity under different platoon sizes without taking string stability as the price, a corresponding tuning function  $\gamma$  is required so that CACPC can be applied under different platoon sizes. Based on the reasons above, a numerical analysis is conducted to obtain the combination of  $\gamma_{acc}$  and  $\gamma_{cacc}$ , which can maintain the string stability of the CACC platoon under different platoon sizes. The results are shown in Fig. 9, where the transparent grey planes represent the string stability margin planes, and the colored surfaces indicate the amplitudes under different  $\gamma_{acc}$  and  $\gamma_{cacc}$ . Moreover, the black curves denote the intersections of the string stability margin plane and the amplitude surface, which are the margin stable combinations of  $\gamma_{acc}$  and  $\gamma_{cacc}$ . In addition, the amplitude of the Y-axis refers to the amplification of the amplitude after the perturbation propagates through the CACC platoon, where amplitude  $\leq 1$  means the CACC platoon is string stable; otherwise, it is string unstable. It is worth noting that Fig. 9 is carried out at the frequency of  $10^{-5}$  Hz, and further exploration that covers a broader frequency domain is carried out in Section V-A.

We can conclude from Fig. 9 that the intersection of the transparent plane and string stability's surface is the basis for selecting  $\gamma_{acc}$  and  $\gamma_{cacc}$ , which can ensure string stability and tap the advantages of CACPC as much as possible. However, the above margin stability curve can not be expressed explicitly analytically. Therefore, by the curve fitting method, we can get the expression of the intersection as follows (since any  $\gamma$  can meet the string stability at platoon size = 5, there is no corresponding expression.):

$$\gamma_{cacc} = \begin{cases} -0.0501 * \gamma_{acc} + 0.2221, & \text{if } n = 2 \\ -0.0248 * \gamma_{acc} + 0.5815, & \text{if } n = 3 \\ -0.0165 * \gamma_{acc} + 0.8995, & \text{if } n = 4 \end{cases} \quad (28)$$

Moreover, with the help of the gain-scheduling method, the appropriate tuning function  $\gamma$  that fits the margin stability

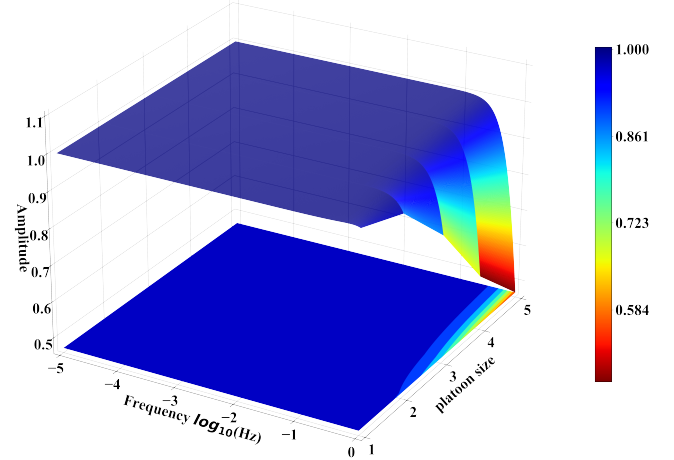


Fig. 10: String stability's surface depends on platoon size.

curve is derived based on the expression above:

$$\gamma_{acc} = \begin{cases} 0, & \text{if } n = 1 \\ 0.4, & \text{if } n = 2 \\ 0.7, & \text{if } n = 3 \\ 0.9, & \text{if } n = 4 \\ 1, & \text{if } n = 5 \end{cases}, \quad (29)$$

$$\gamma_{cacc} = \begin{cases} 0, & \text{if } n = 1 \\ 0.3, & \text{if } n = 2 \\ 0.6, & \text{if } n = 3 \\ 0.9, & \text{if } n = 4 \\ 1, & \text{if } n = 5 \end{cases}, \quad (30)$$

where  $n$  denotes platoon size.

## V. NUMERICAL ANALYSES

In this section, we first validate the string stability of CACPC based on the theoretical result derived in Section IV by numerical simulation. Then a series of simulation experiments are conducted to explore the impact of YK parameterization on dynamic performance.

### A. Validation of string stability

Based on the results in Section IV-B and IV-C, we have obtained the amplitude of CACPC under different platoon sizes. It is necessary to keep the string stable to prevent the perturbation from being amplified during propagation. Therefore, a numerical experiment is conducted to explore the string stability of the CACC platoon under low frequency ( $10^{-5} - 10^0$  Hz). Fig. 10 shows the result where the curved surface represents the amplitude of the CACC platoon under low frequency ( $10^{-5} - 10^0$  Hz) and different platoon sizes, and the bottom plane is the projection of the curved surface. Besides, the amplitude of the Y-axis is the amplification of the amplitude after the interference propagates through the CACC platoon, where amplitude  $\leq 1$  means that the CACC platoon is string stable; otherwise, it is string unstable.

Fig. 10 shows that the string stability surface of the CACPC is below 1 for different frequencies and platoon sizes, indicating that the CACPC proposed above can avoid amplifying perturbation. Therefore, one conclusion can be drawn that the CACPC can ensure string stability under different platoon sizes.

### B. Simulation experiments of YK parameterization

Unlike theoretical analyses, behaviors observed in simulation experiments are closer to those in the real traffic environment. In order to further explore the actual effect of the controller switching using the YK parameterization, a series of simulation experiments are carried out based on CACPC as a supplement to the theoretical analysis. It should be noted that for the cases without YK parameterization, since there is no adaptive platoon size control strategy, the fixed platoon control strategy, i.e. it only functions when the platoon size reaches the specified platoon size.

1) *Simulation experiments maintain a constant speed during the forming and splitting process:*

*Simulation scenario:* The simulation scenario is set as follows: at first, a leader vehicle drives on an infinitely long road under a given speed and acceleration configuration (containing five same small perturbations that occurred at the simulation time of 300s, 1000s, 1700s, 2400s, and 3100s under different platoon size). There are four experiments conducted:

- 1) *Experiment I:* The forming process of the CACC platoon with YK parameterization where an ACC (which is a CACC but degraded to an ACC functionally) follows the leader at the beginning, and more CACCs join the CACC platoon one by one at the simulation time of 700s, 1400s, 2100s, and 2800s.
- 2) *Experiment II:* The forming process of the CACC platoon without YK parameterization where an ACC (which is a CACC but degraded to an ACC functionally) follows the leader at the beginning, and more CACCs join the CACC platoon one by one at the simulation time of 700s, 1400s, 2100s, and 2800s. Note that since the fixed platoon control only functions when the platoon size reaches 5, the platoon control without YK parameterization is enabled after 2800s.
- 3) *Experiment III:* The splitting process of the CACC platoon with YK parameterization where an ACC (which is a CACC but degraded to an ACC functionally) and four CACCs follow the leader at the beginning, and the last CACC in the platoon leaves one by one at the simulation time of 700s, 1400s, 2100s, and 2800s.
- 4) *Experiment IV:* The splitting process of the CACC platoon without YK parameterization where an ACC (which is a CACC but degraded to an ACC functionally) and four CACCs follow the leader at the beginning, and the last CACC in the platoon leaves one by one at the simulation time of 700s, 1400s, 2100s, and 2800s. Note that since the fixed platoon control only functions when the platoon size reaches 5, the platoon control without YK parameterization is enabled before 700s.

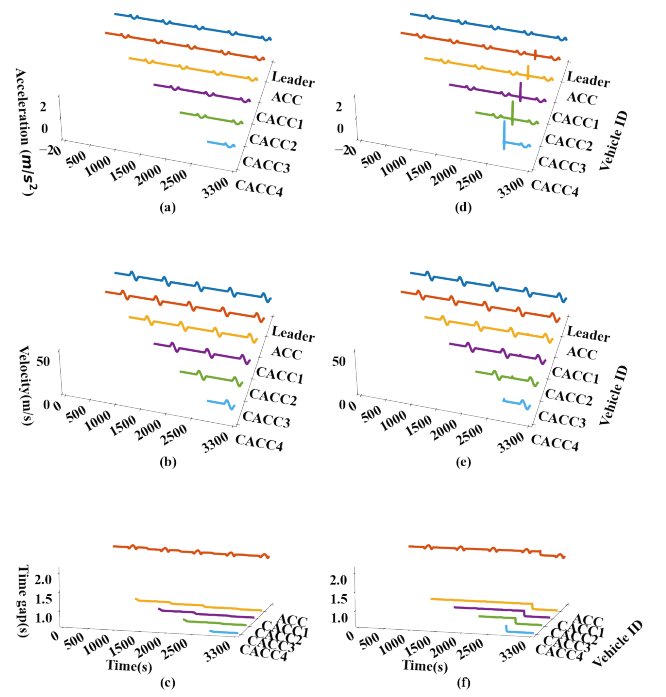


Fig. 11: Simulation results of experiment I and II: CACPC with or without YK parameterization under the platoon forming case. (a)-(c) show the simulation results of experiment I, and (d)-(f) show the simulation results of experiment II. (a),(d) Acceleration of simulation results; (b),(e) Velocity of simulation results; (c),(f) Time gap of simulation results.

The first pair of experiments is the forming process of the CACC platoon, where an ACC (which is a CACC but degraded to an ACC functionally) follows the leader at the beginning, and more CACCs join the CACC platoon one by one at the simulation time of 700s, 1400s, 2100s, and 2800s. Moreover, periodic perturbations are applied to the leader to explore the string stability of the CACC platoon under different platoon sizes. Another pair of experiments are conducted, simulating the splitting process of the CACC platoon. It should be noted that there are four experiments conducted to analyze the impact of the YK parameterization under the platoon forming case and the platoon splitting case. Experiment I and III applies YK parameterization with the tuning function  $\gamma$  proposed above, while experiment II and IV switch to the platoon control mode directly only the platoon size reaches maximum platoon size  $S = 5$ .

*Simulation results.* Fig. 11 and 13 show the results of experiments I, II, III and IV, respectively. Moreover, Fig. 12 and 14 show the detailed perturbation simulation results of experiments I, II, III and IV. In Fig. 11 and 13, (a)-(c) show the simulation results of the case with YK parameterization and (d)-(f) show the simulation results of the case without YK parameterization where (a),(d) Acceleration of simulation results; (b),(e) Velocity of simulation results; (c),(f) Time gap of simulation results. As for Fig. 12 and 14, (a)-(e) show

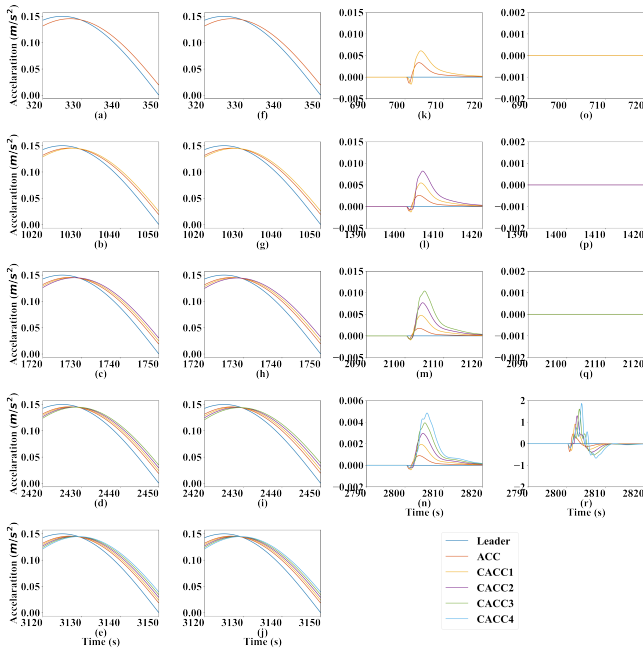


Fig. 12: Detailed perturbation simulation results of experiments I and II: CACPC with or without YK parameterization under the platoon forming case. For experiment I, (a)-(e) show the propagating processes of five applied perturbations, and (k)-(n) show the four switching processes. For experiment II, (f)-(j) show the propagating processes of five applied perturbations, and (o)-(r) show the four switching processes.

the propagating processes of five applied perturbations and (f)-(i) show the four switching processes of the case with YK parameterization. Furthermore, for the case without YK parameterization, (j)-(n) show the propagating processes of five applied perturbations, and (o)-(r) show the four switching processes.

In Fig. 11 and 12, the process of the gradual formation of the CACC platoon with and without YK parameterization is clearly shown, while the process of the gradual splitting is shown in Fig. 13 and 14. The first attention is spontaneous perturbations during controller switching. From the comparison of Fig. 12 and 14, we can find that the controller switching causes spontaneous perturbations in the process of platoon formation, which is caused by the changing of the equivalent desired time gap. These spontaneous perturbations can be suppressed by applying the tuning function  $\gamma$  to achieve smooth switching. Specifically, the maximum magnitude of the perturbation is reduced from  $2m/s^2$  to  $0.011m/s^2$  by YK parameterization. However, in the case without YK parameterization, due to the direct switching when the platoon size reaches or leaves the trigger size, the spontaneous perturbation is significant, which seriously impacts the stability and safety of the traffic flow. The second attention is string stability. All CACPCs applied under different CACC platoon sizes can maintain string stability through YK parameterization which are shown in Fig. 12 and 14. Furthermore, the subplots of the time gap in Fig. 11 and 13 illustrate that with YK parameterization, the time gap decreases as the platoon size increases. However, without YK

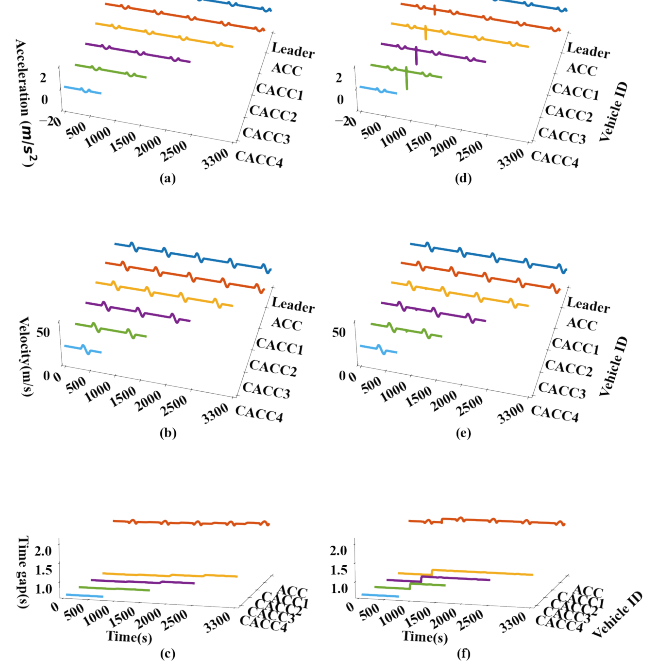


Fig. 13: Simulation results of experiments III and IV: CACPC with or without YK parameterization under the platoon splitting case. (a)-(c) show the simulation results of experiment III, and (d)-(f) show the simulation results of experiment IV. (a),(d) Acceleration of simulation results; (b),(e) Velocity of simulation results; (c),(f) Time gap of simulation results.

parameterization, the time gap does not change significantly with the change in platoon size unless the specified platoon size is reached. Therefore, it can be concluded that with YK parameterization, the platoon control mode can be effective regardless of the platoon size so that it does not limit the gain of CACCs for traffic flow.

Moreover, YK parameterization can work under any CACC MPR since it can be applied even in a typical scenario where the CACC MPR is low and the platoon size is small. Nevertheless, for the case without YK parameterization, the CACPCs do not function sufficiently until the set trigger platoon size is reached, which means it is hard to function for a long period because there will be a long time until the CACC MPR gets high. In addition, because the splitting and forming processes are similar, the following simulation experiments are only conducted in the forming process. Notice that from the difference in the acceleration between subplot (a) and (b) in Fig. 11 and 13, which is detailed shown in subplot (k)-(r) in Fig. 12 and 14, a misunderstood conclusion can be drawn because the perturbation is amplified with or without YK parameterization. However, the perturbation is caused by the equivalent desired time gap increase during the controller switching. In the case with YK parameterization, the perturbation only rises once and then back to the equivalent state. On the contrary, for the case without YK parameterization, the

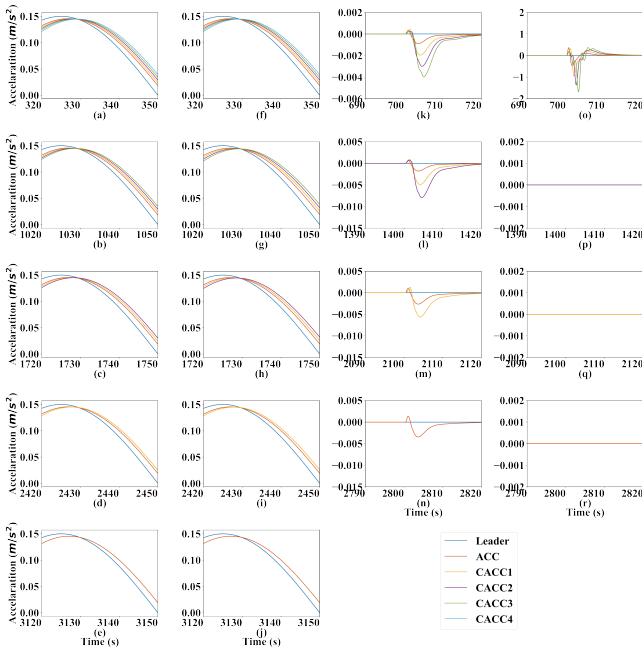


Fig. 14: Detailed perturbation simulation results of experiments III and IV: CACPC with or without YK parameterization under the platoon splitting case. For experiment III, (a)-(e) show the propagating processes of five applied perturbations, and (k)-(n) show the four switching processes. For experiment IV, (f)-(j) show the propagating processes of five applied perturbations, and (o)-(r) show the four switching processes.

perturbation fluctuates during the propagating process, which means the switching progress is not smooth enough to suppress the perturbation.

2) *Simulation experiments maintain a fluctuating speed during the forming process:*

**Simulation scenario:** The simulation scenario is similar to experiment I in Section V-B1, but different in the given speed and acceleration configuration of the leader vehicle. In this simulation experiment, the speed of the leader vehicle fluctuates all the time to simulate the traffic oscillation scenario. There are two experiments conducted:

- 1) *Experiment V:* The forming process of the CACC platoon with YK parameterization under the fluctuating velocity case where an ACC (which is a CACC but degraded to an ACC functionally) follows the leader at the beginning, and more CACCs join the CACC platoon one by one at the simulation time of 700s, 1400s, 2100s, and 2800s.
- 2) *Experiment VI:* The forming process of the CACC platoon without YK parameterization under the fluctuating velocity case where an ACC (which is a CACC but degraded to an ACC functionally) follows the leader at the beginning, and more CACCs join the CACC platoon one by one at the simulation time of 700s, 1400s, 2100s, and 2800s. Note that since the fixed platoon control only functions when the platoon size reaches 5, the platoon control without YK parameterization is enabled after 2800s.

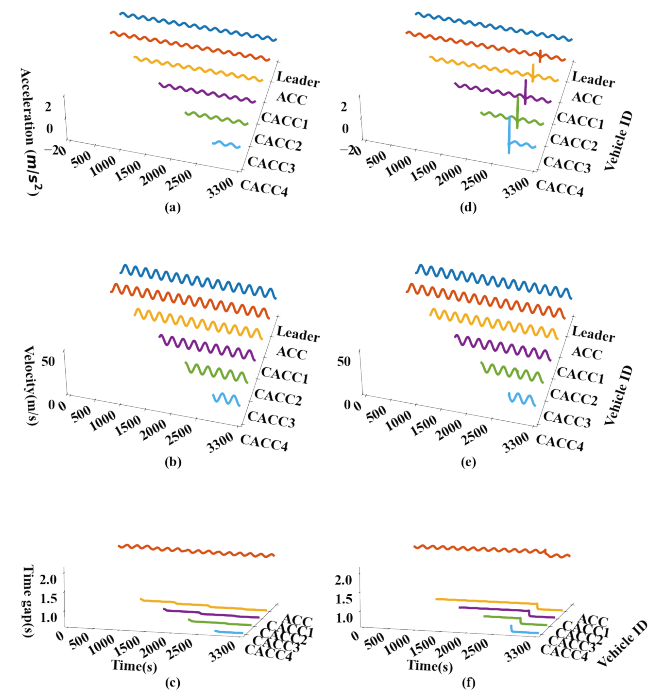


Fig. 15: Simulation results of experiments V and VI: CACPC with or without YK parameterization under the fluctuating velocity case. (a)-(c) show the simulation results of experiment V, and (d)-(f) show the simulation results of experiment VI. (a),(d) Acceleration of simulation results; (b),(e) Velocity of simulation results; (c),(f) Time gap of simulation results.

**Simulation results.** Fig. 15, 16 show the results of experiments V and VI from global and local perspectives, respectively. The formats of Fig. 15, 16 are same as Fig. 11, 12. For the sake of simplicity, the detailed introduction is omitted. In Fig. 15, the top graph plots the vehicles' accelerations, the median graph plots the vehicles' velocities during the simulation, and the bottom graph plots the time gap during the simulation in each figure.

From Fig. 15, the simulation results under the traffic oscillation scenario are similar to the results with constant velocity. The corresponding detailed simulation results are shown in Fig. 16. The spontaneous perturbations caused by the controller switching are not significant and have the magnitude of  $0.015 \text{ m/s}^2$  with the YK parameterization, while the perturbation has the magnitude of  $2.15 \text{ m/s}^2$  for the case without YK parameterization under the traffic oscillation scenario. Moreover, a noticeable rise appears in the acceleration subplots, which significantly negatively impacts traffic safety. A conclusion can be drawn that adopting YK parameterization can ensure the smooth switching of the controllers while not adopting it does not, whether it is traffic oscillation or equilibrium state.

3) *Simulation experiments maintain a constant speed during the multiple CACCs forming processes:*

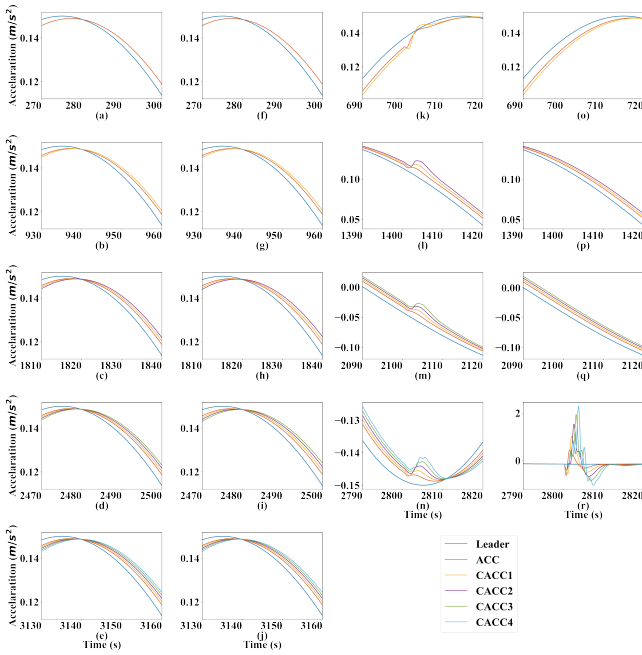


Fig. 16: Detailed perturbation simulation results of experiments V and VI: CACPC with or without YK parameterization under the fluctuating velocity case. For experiment V, (a)-(e) show the propagating processes of five applied perturbations, and (k)-(l) show the four switching processes. For experiment VI, (f)-(j) show the propagating processes of five applied perturbations, and (o)-(r) show the four switching processes.

**Simulation scenario:** The simulation scenario of experiment VII is set as follows: at first, a leader vehicle drives on an infinitely long road under a given speed and acceleration configuration, which is similar to experiment I in Section V-B1. There are only three perturbations at the simulation time of 300s, 1000s, and 1700s. Moreover, the forming process of the CACC platoon is that two CACCs join the ACC platoon at the same time, and the forming process repeats twice at the simulation time of 700s and 1400s. Notice that only the case with YK parameterization applied is simulated here because simulation results of the case without YK parameterization are similar to experiment II in Section V-B1.

**Simulation results.** Fig. 17 shows the results of experiment VII. In the left subplot, the top graph plots the vehicles' accelerations, the median graph plots the vehicles' velocities during the simulation, and the bottom graph plots the time gap during the simulation. Moreover, the right subplot shows the detailed acceleration in 690-720s and 1390-1420s to explore the spontaneous perturbation during controllers switching.

From Fig. 17, the first conclusion can be drawn that YK parameterization can keep string stability even during the multiple CACCs forming process. The second conclusion can be found in Fig. 17 (d) and (e) that the spontaneous perturbation caused by controllers switching is amplified with multiple CACCs forming. However, the magnitude of the first switching perturbation is still only  $0.015 \text{ m/s}^2$ , which is significantly lower than the case without YK parameterization.

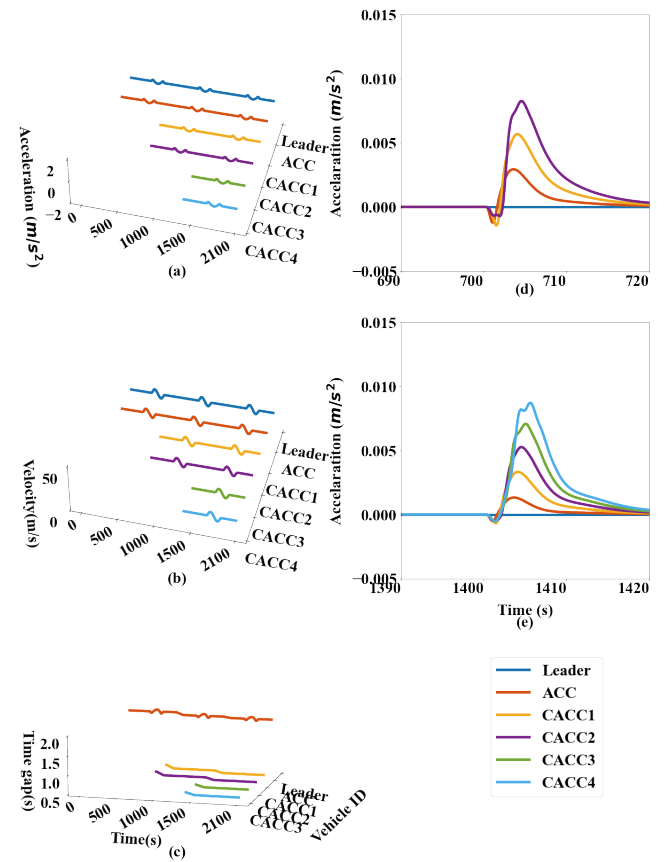


Fig. 17: Simulation results of experiment VII: CACPC with YK parameterization under multiple CACCs forming at the same time. (a) Acceleration of simulation results; (b) Velocity of simulation results; (c) Time gap of simulation results; (d) Detailed acceleration of simulation results in 690-720s; (e) Detailed acceleration of simulation results in 1390-1420s

## VI. CONCLUSION

This paper proposes a switching control model called CACPC to improve the capability by treating the entire CACC platoon as the control object instead of a single vehicle and switching the control as the platoon size changes. In this control model, the string stability of the CACC platoon is analyzed to obtain the margin time gap for different platoon sizes. Then the YK parameterization is applied to ensure the string stability of the CACC platoon when switching between different control modes, and the corresponding tuning function is proposed so that the application of this control mode is not limited by the fixed platoon size. In addition, the effect of YK parameterization on the dynamic performance of CACPC is explored. The following conclusions can be drawn from this paper:

- 1) A new switching control mode for the CACC platoon is proposed capable of adaptively controlling the CACC platoon with different platoon sizes.
- 2) CACPC consists of two sets of CACC controllers. YK parameterization ensures stable coupling of the two sets of controllers before and after controller switching to



Fig. 18: Field experiment scene.

guarantee smooth switching and string stability at different platoon sizes.

- 3) The specific process of CACPC control design is given and the corresponding CACPC controller design is carried out.
- 4) Combination of tuning function  $\gamma$  under different platoon sizes is derived by ensuring that the application range of CACPC is not limited by platoon size.
- 5) Adopting YK parameterization can significantly suppress the spontaneous perturbation from  $2m/s^2$  to  $0.011m/s^2$  caused by the controller switch.
- 6) YK parameterization can ensure smooth controller switching under the equilibrium state, traffic oscillation, and multiple CACCs forming.

#### APPENDIX A. SYSTEM IDENTIFICATION OF LOWER LEVEL CONTROLLER BASED ON FIELD EXPERIMENTS

*Experiment preparation:* The experiment was conducted at the Closed test site of National Smart CAV & C-ITS (Beijing + Hebei) Demonstration Zone Shunyi Base on March 29, 2021. Two cycabs were used for the experiment: autonomous driving vehicles developed by the iDriverplus technology company. The scheme of LiDAR+ millimeter wave + Ultrasonic radar + GPS inertial navigation was adopted as the navigation system, and the distance measurement accuracy is 0.05m. The decision frequency is 20 Hz which equals a 50ms decision interval. Fig. 18 shows the scene of the field experiment.

*Experiment scheme:* The experiments were divided into 5 groups. Each group had several rounds, which amounted to a total of 21 rounds of experiments. In each round, the front car drove in accordance with the speed configuration, while the back car used the longitudinal control of the ACC system to follow the front car and record the actual acceleration of the back car. Different groups used different control parameters of

TABLE II: Parameters chosen for different experiment groups.

| Index of experiments group | $k_p$       | $k_d$     | $h_i$ | round |
|----------------------------|-------------|-----------|-------|-------|
| 1 <sup>st</sup>            | $0.7s^{-2}$ | $0s^{-1}$ | 2 s   | 2     |
| 2 <sup>nd</sup>            | $0.5s^{-2}$ | $0s^{-1}$ | 1.8 s | 5     |
| 3 <sup>rd</sup>            | $0.6s^{-2}$ | $0s^{-1}$ | 2 s   | 7     |
| 4 <sup>th</sup>            | $0.7s^{-2}$ | $0s^{-1}$ | 2 s   | 4     |
| 5 <sup>th</sup>            | $0.4s^{-2}$ | $0s^{-1}$ | 2 s   | 3     |

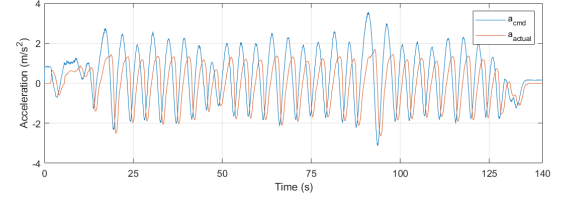


Fig. 19: Experiment data of the command acceleration and the actual acceleration in first round, where  $a_{cmd}$  means the command acceleration and  $a_{actual}$  means the actual acceleration.

the ACC system to ensure that a general conclusion could be drawn.

The control parameters of the ACC system in different experimental groups are shown in communication, and the specific parameter setting is shown in Table. II.

The experiment data of command acceleration and actual acceleration in the first round are shown in Fig. 19, where  $a_{cmd}$  means the command acceleration and  $a_{actual}$  means the actual acceleration.

In order to calibrate the transfer function of the lower controller  $G_i(s)$ , the command acceleration and actual acceleration of the back car in each round are regarded as input and output respectively. Notice that since the output of the lower controller  $G_i(s)$  in Fig. 2 is position instead of acceleration, additional second-order integration is applied. Using the System Identification toolbox in MATLAB and setting the desired system type, the transfer function is fitted as follows:

$$G_i(s) = \frac{k_G}{s^2(\tau_i s + 1)} e^{-\phi_i s} = \frac{0.9403}{s^2(0.7862s + 1)} e^{-0.2s}, \quad (31)$$

which keeps fit error to minimum: FPE=0.08699 and MSE=0.0868.

#### APPENDIX B. PROOF OF THE EQUATION (17-18)

The Equation (17-18) must satisfy the following identities:

$$\begin{aligned} 1) \quad G &= NM^{-1} = \tilde{M}^{-1}\tilde{N}, \\ 2) \quad K_i &= U_i V_i^{-1} = \tilde{V}_i^{-1}\tilde{U}_i, \\ 3) \quad &\left[ \begin{array}{cc} \tilde{V}_i & -\tilde{U}_i \\ -\tilde{N} & \tilde{M} \end{array} \right] \left[ \begin{array}{cc} M & U_i \\ N & V_i \end{array} \right] \\ &= \left[ \begin{array}{cc} M & U_i \\ N & V_i \end{array} \right] \left[ \begin{array}{cc} \tilde{V}_i & -\tilde{U}_i \\ -\tilde{N} & \tilde{M} \end{array} \right] \\ &= \left[ \begin{array}{cc} I & 0 \\ 0 & I \end{array} \right]. \end{aligned}$$

**Proof.** Proof of (a)  $G = \tilde{M}^{-1}\tilde{N}$ :

$$\tilde{M}^{-1}\tilde{N}$$

$$\begin{aligned}
&= \left[ \begin{array}{cc|cc} A + BD_i^c C & BC_i^c & BD_i^c & \\ B_i^c C & A_i^c & B_i^c & \\ \hline C & -F_i^c & I & \end{array} \right]^{-1} \left[ \begin{array}{cc|c} A + BD_i^c C & BC_i^c & B \\ B_i^c C & A_i^c & 0 \\ \hline C & -F_i^c & 0 \end{array} \right] \\
&= \left[ \begin{array}{cc|cc} A & B(C_i^c + D_i^c F_i^c) & -BD_i^c & \\ 0 & A_i^c + B_i^c F_i^c & -B_i^c & \\ \hline C & -F_i^c & I & \end{array} \right] \left[ \begin{array}{cc|c} A + BD_i^c C & BC_i^c & B \\ B_i^c C & A_i^c & 0 \\ \hline C & -F_i^c & 0 \end{array} \right] \\
&= \left[ \begin{array}{cc|cc} A & B(C_i^c + D_i^c F_i^c) & -BD_i^c C & BD_i^c F_i^c & 0 \\ 0 & A_i^c + B_i^c F_i^c & -B_i^c C & B_i^c F_i^c & 0 \\ 0 & 0 & A + BD_i^c C & BC_i^c & B \\ 0 & 0 & B_i^c C & A_i^c & 0 \\ \hline C & -F_i^c & C & -F_i^c & 0 \end{array} \right] \\
&= \left[ \begin{array}{cc|cc|c} A & B(C_i^c + D_i^c F_i^c) & 0 & 0 & B \\ 0 & A_i^c + B_i^c F_i^c & 0 & 0 & 0 \\ 0 & 0 & A + BD_i^c C & BC_i^c & B \\ 0 & 0 & B_i^c C & A_i^c & 0 \\ \hline C & -F_i^c & 0 & 0 & 0 \end{array} \right] \\
&= \left[ \begin{array}{c|c} A & B \\ C & 0 \end{array} \right], \tag{32}
\end{aligned}$$

where  $\mathbf{T} = \begin{bmatrix} \mathbf{I} & 0 & -\mathbf{I} & 0 \\ 0 & \mathbf{I} & 0 & -\mathbf{I} \\ 0 & 0 & \mathbf{I} & 0 \\ 0 & 0 & 0 & \mathbf{I} \end{bmatrix}$ ,  $\mathbf{T}^{-1} = \begin{bmatrix} \mathbf{I} & 0 & \mathbf{I} & 0 \\ 0 & \mathbf{I} & 0 & \mathbf{I} \\ 0 & 0 & \mathbf{I} & 0 \\ 0 & 0 & 0 & \mathbf{I} \end{bmatrix}$  is adopted in the similarity transformation. The proofs that  $G = NM^{-1}$  and (ii) are analogous.

**Proof.** Proof of (c)  $\left[ \begin{array}{cc} M & U_i \\ N & V_i \end{array} \right] \left[ \begin{array}{cc} \tilde{V}_i & -\tilde{U}_i \\ -\tilde{N} & \tilde{M} \end{array} \right] = \left[ \begin{array}{cc} I & 0 \\ 0 & I \end{array} \right]$ .

$$\begin{aligned}
&\left[ \begin{array}{cc} M & U_i \\ N & V_i \end{array} \right]^{-1} \\
&= \left[ \begin{array}{cc|cc} A + BF & 0 & -B & 0 \\ 0 & A_i^c + B_i^c F_i^c & 0 & B_i^c \\ \hline -F & C_i^c + D_i^c F_i^c & I & D_i^c \\ -C & F_i^c & 0 & I \end{array} \right]^{-1} \tag{33} \\
&= \left[ \begin{array}{cc|cc} A + BD_i^c C & BC_i^c & -B & BD_i^c \\ B_i^c C & A_i^c & 0 & B_i^c \\ \hline F_i - D_i^c C & -C_i^c & I & -D_i^c \\ C & -F_i^c & 0 & I \end{array} \right] \\
&= \left[ \begin{array}{cc} \tilde{V}_i & -\tilde{U}_i \\ -\tilde{N} & \tilde{M} \end{array} \right].
\end{aligned}$$

Q.E.D.

#### ACKNOWLEDGMENT

This research was sponsored by National Science Foundation of China (No. 51878161, No. 71931002, No.72288101 and No.52072067).

#### REFERENCES

- [1] Z. Wang, Y. Bian, S. E. Shladover, G. Wu, S. E. Li, and M. J. Barth, "A survey on cooperative longitudinal motion control of multiple connected and automated vehicles," *IEEE Intelligent Transportation Systems Magazine*, vol. 12, no. 1, pp. 4–24, 2019.
- [2] J. Ploeg, B. T. Scheepers, E. Van Nunen, N. Van de Wouw, and H. Nijmeijer, "Design and experimental evaluation of cooperative adaptive cruise control," in *2011 14th International IEEE Conference on Intelligent Transportation Systems (ITSC)*. IEEE, 2011, pp. 260–265.
- [3] L. Zhou, T. Ruan, K. Ma, C. Dong, and H. Wang, "Impact of cav platoon management on traffic flow considering degradation of control mode," *Physica A: Statistical Mechanics and its Applications*, p. 126193, 2021.
- [4] J. Vander Werf, S. E. Shladover, M. A. Miller, and N. Kourjanskaia, "Effects of adaptive cruise control systems on highway traffic flow capacity," *Transportation Research Record*, vol. 1800, no. 1, pp. 78–84, 2002.
- [5] L. L. C. Verizon North, "Federal Communications Commission," *Proceeding Number*, vol. 19, p. 354, 2020.
- [6] S. Gong and L. Du, "Cooperative platoon control for a mixed traffic flow including human drive vehicles and connected and autonomous vehicles," *Transportation research part B: methodological*, vol. 116, pp. 25–61, 2018.
- [7] C. Wang, S. Gong, A. Zhou, T. Li, and S. Peeta, "Cooperative adaptive cruise control for connected autonomous vehicles by factoring communication-related constraints," *Transportation Research Part C: Emerging Technologies*, vol. 113, pp. 124–145, 2020.
- [8] H. Liu, X. Kan, S. E. Shladover, X.-Y. Lu, and R. E. Ferlis, "Impact of cooperative adaptive cruise control on multilane freeway merge capacity," *Journal of Intelligent Transportation Systems*, vol. 22, no. 3, pp. 263–275, 2018.
- [9] L. Xiao, M. Wang, W. Schakel, and B. van Arem, "Unravelling effects of cooperative adaptive cruise control deactivation on traffic flow characteristics at merging bottlenecks," *Transportation research part C: emerging technologies*, vol. 96, pp. 380–397, 2018.
- [10] P. Bansal and K. M. Kockelman, "Forecasting Americans' long-term adoption of connected and autonomous vehicle technologies," *Transportation Research Part A: Policy and Practice*, vol. 95, pp. 49–63, 2017.
- [11] T. Ruan, H. Wang, L. Zhou, Y. Zhang, C. Dong, and Z. Zuo, "Impacts of Information Flow Topology on Traffic Dynamics of CAV-MV Heterogeneous Flow," *IEEE Transactions on Intelligent Transportation Systems*, pp. 1–16, 2022.
- [12] Z. Yao, T. Xu, Y. Jiang, and R. Hu, "Linear stability analysis of heterogeneous traffic flow considering degradations of connected automated vehicles and reaction time," *Physica A: Statistical Mechanics and its Applications*, vol. 561, 2021.
- [13] Y. Qin, H. Wang, and B. Ran, "Stability analysis of connected and automated vehicles to reduce fuel consumption and emissions," *Journal of Transportation Engineering, Part A: Systems*, vol. 144, no. 11, p. 04018068, 2018.
- [14] T. Ruan, L. Zhou, and H. Wang, "Stability of heterogeneous traffic considering impacts of platoon management

- with multiple time delays,” *Physica A: Statistical Mechanics and its Applications*, vol. 583, p. 126294, 2021.
- [15] M. Wang, “Infrastructure assisted adaptive driving to stabilise heterogeneous vehicle strings,” *Transportation Research Part C: Emerging Technologies*, vol. 91, pp. 276–295, 2018.
- [16] J. Sun, Z. Zheng, and J. Sun, “Stability analysis methods and their applicability to car-following models in conventional and connected environments,” *Transportation research part B: methodological*, vol. 109, pp. 212–237, 2018.
- [17] J. Ploeg, N. Van De Wouw, and H. Nijmeijer, “L<sub>p</sub> string stability of cascaded systems: Application to vehicle platooning,” *IEEE Transactions on Control Systems Technology*, vol. 22, no. 2, pp. 786–793, 2013.
- [18] H. Wang, Y. Qin, W. Wang, and J. Chen, “Stability of cacc-manual heterogeneous vehicular flow with partial cacc performance degrading,” *Transportmetrica B: Transport Dynamics*, vol. 7, no. 1, pp. 788–813, 2019.
- [19] Y. Qin, H. Wang, and D. Ni, “Lighthill-whitham-richards model for traffic flow mixed with cooperative adaptive cruise control vehicles,” *Transportation Science*, vol. 55, no. 4, pp. 883–907, 2021.
- [20] F. Navas, V. Milanés, and F. Nashashibi, “Using plug&play control for stable acc-cacc system transitions,” in *2016 IEEE Intelligent Vehicles Symposium (IV)*. IEEE, 2016, pp. 704–709.
- [21] M. Montanino and V. Punzo, “On string stability of a mixed and heterogeneous traffic flow: A unifying modelling framework,” *Transportation Research Part B: Methodological*, vol. 144, pp. 133–154, 2021, publisher: Elsevier Ltd. [Online]. Available: <https://doi.org/10.1016/j.trb.2020.11.009>
- [22] M. Shang and R. E. Stern, “Impacts of commercially available adaptive cruise control vehicles on highway stability and throughput,” *Transportation Research Part C: Emerging Technologies*, vol. 122, p. 102897, 2021, publisher: Pergamon.
- [23] G. Marsden, M. McDonald, and M. Brackstone, “Towards an understanding of adaptive cruise control,” *Transportation Research Part C: Emerging Technologies*, vol. 9, no. 1, pp. 33–51, 2001.
- [24] J. Wang, L. Lu, and S. Peeta, “Real-time deployable and robust cooperative control strategy for a platoon of connected and autonomous vehicles by factoring uncertain vehicle dynamics,” *Transportation Research Part B: Methodological*, vol. 163, pp. 88–118, Sep. 2022.
- [25] J. Shen, E. K. H. Kammara, and L. Du, “Fully Distributed Optimization based CAV Platooning Control under Linear Vehicle Dynamics,” Mar. 2021, arXiv:2103.11081 [math].
- [26] L. Xu, W. Zhuang, G. Yin, and C. Bian, “Energy-oriented cruising strategy design of vehicle platoon considering communication delay and disturbance,” *Transportation Research Part C: Emerging Technologies*, vol. 107, pp. 34–53, Oct. 2019.
- [27] Y. Qin, H. Wang, and D. Ni, “Lighthill-Whitham-Richards Model for Traffic Flow Mixed with Cooperative Adaptive Cruise Control Vehicles,” *Transportation Science*, vol. 55, no. 4, pp. 883–907, Jul. 2021. [Online]. Available: <http://pubsonline.informs.org/doi/10.1287/trsc.2021.1057>
- [28] Y. Zhou, S. Ahn, M. Wang, and S. Hoogendoorn, “Stabilizing mixed vehicular platoons with connected automated vehicles: An h-infinity approach,” *Transportation Research Part B: Methodological*, vol. 132, pp. 152–170, 2020.
- [29] M. Stefanovic and M. G. Safonov, “Safe Adaptive Switching Control: Stability and Convergence,” *IEEE Transactions on Automatic Control*, vol. 53, no. 9, pp. 2012–2021, Oct. 2008. [Online]. Available: <http://ieeexplore.ieee.org/document/4639465/>
- [30] K. C. Dey, L. Yan, X. Wang, Y. Wang, H. Shen, M. Chowdhury, L. Yu, C. Qiu, and V. Soundararaj, “A review of communication, driver characteristics, and controls aspects of cooperative adaptive cruise control (cacc),” *IEEE Transactions on Intelligent Transportation Systems*, vol. 17, no. 2, pp. 491–509, 2015.
- [31] F. Navas and V. Milanés, “Mixing v2v-and non-v2v-equipped vehicles in car following,” *Transportation research part C: emerging technologies*, vol. 108, pp. 167–181, 2019.
- [32] S. Stüdli, M. M. Seron, and R. H. Middleton, “From vehicular platoons to general networked systems: String stability and related concepts,” *Annual Reviews in Control*, vol. 44, pp. 157–172, 2017.
- [33] Y. Qin and H. Wang, “Analytical framework of string stability of connected and autonomous platoons with electronic throttle angle feedback,” *Transportmetrica A: Transport Science*, vol. 17, no. 1, pp. 59–80, 2021.
- [34] M. Montanino, J. Monteil, and V. Punzo, “From homogeneous to heterogeneous traffic flows: L<sub>p</sub> string stability under uncertain model parameters,” *Transportation Research Part B: Methodological*, vol. 146, pp. 136–154, 2021.
- [35] I. G. Jin and G. Orosz, “Dynamics of connected vehicle systems with delayed acceleration feedback,” *Transportation Research Part C: Emerging Technologies*, vol. 46, pp. 46–64, 2014.
- [36] V. Milanés and S. E. Shladover, “Modeling cooperative and autonomous adaptive cruise control dynamic responses using experimental data,” *Transportation Research Part C: Emerging Technologies*, vol. 48, pp. 285–300, 2014.
- [37] V. Milanés, S. E. Shladover, J. Spring, C. Nowakowski, H. Kawazoe, and M. Nakamura, “Cooperative adaptive cruise control in real traffic situations,” *IEEE Transactions on intelligent transportation systems*, vol. 15, no. 1, pp. 296–305, 2013.
- [38] Y. Zhang, Y. Bai, J. Hu, and M. Wang, “Control design, stability analysis, and traffic flow implications for cooperative adaptive cruise control systems with compensation of communication delay,” *Transportation Research Record*, vol. 2674, no. 8, pp. 638–652, 2020.
- [39] G. b. Orosz, J. Moehlis, and F. Bullo, “Delayed car-following dynamics for human and robotic drivers,” in

- International Design Engineering Technical Conferences and Computers and Information in Engineering Conference*, vol. 54815, 2011, pp. 529–538.
- [40] M. Montanino and V. Punzo, “On string stability of a mixed and heterogeneous traffic flow: A unifying modelling framework,” *Transportation Research Part B: Methodological*, vol. 144, pp. 133–154, 2021.
- [41] S. Feng, Y. Zhang, S. E. Li, Z. Cao, H. X. Liu, and L. Li, “String stability for vehicular platoon control: Definitions and analysis methods,” *Annual Reviews in Control*, vol. 47, pp. 81–97, 2019.
- [42] D. Swaroop, “String stability of interconnected systems: An application to platooning in automated highway systems,” 1994.
- [43] S. Darbha, “On the synthesis of controllers for continuous time LTI systems that achieve a non-negative impulse response,” *Automatica*, vol. 39, no. 1, pp. 159–165, 2003.
- [44] S. Stüdli, M. M. Seron, and R. H. Middleton, “From vehicular platoons to general networked systems: String stability and related concepts,” *Annual Reviews in Control*, vol. 44, no. 2, pp. 157–172, 2017.
- [45] S. Dasgupta and B. D. Anderson, “A parametrization for the closed-loop identification of nonlinear time-varying systems,” *Automatica*, vol. 32, no. 10, pp. 1349–1360, 1996.
- [46] F. Navas, V. Milanés, and F. Nashashibi, “Youla-kucera based online closed-loop identification for longitudinal vehicle dynamics,” in *2017 21st International Conference on System Theory, Control and Computing (ICSTCC)*. IEEE, 2017, pp. 88–93.
- [47] J. Pommaret and A. Quadrat, “Generalized bezout identity,” *Applicable Algebra in Engineering, Communication and Computing*, vol. 9, no. 2, pp. 91–116, 1998.
- [48] H. Niemann and J. Stoustrup, “An architecture for implementation of multivariable controllers,” in *Proceedings of the 1999 American Control Conference (Cat. No. 99CH36251)*, vol. 6. IEEE, 1999, pp. 4029–4033.
- [49] T.-T. Tay, I. Mareels, and J. B. Moore, *High performance control*. Springer Science & Business Media, 1998.
- [50] I. Mahtout, F. Navas, V. Milanes, and F. Nashashibi, “Advances in youla-kucera parametrization: A review,” *Annual Reviews in Control*, vol. 49, pp. 81–94, 2020.
- [51] G. J. Naus, R. P. Vugts, J. Ploeg, M. J. van De Molengraft, and M. Steinbuch, “String-stable cacc design and experimental validation: A frequency-domain approach,” *IEEE Transactions on vehicular technology*, vol. 59, no. 9, pp. 4268–4279, 2010.
- [52] Y. Bian, Y. Zheng, W. Ren, S. E. Li, J. Wang, and K. Li, “Reducing time headway for platooning of connected vehicles via v2v communication,” *Transportation Research Part C: Emerging Technologies*, vol. 102, pp. 87–105, 2019.
- [53] L. Xiao and F. Gao, “Practical string stability of platoon of adaptive cruise control vehicles,” *IEEE Transactions on intelligent transportation systems*, vol. 12, no. 4, pp. 1184–1194, 2011.
- [54] S. Oncu, J. Ploeg, N. Van De Wouw, and H. Niemeijer, “Cooperative adaptive cruise control: Network-aware analysis of string stability,” *IEEE Transactions on Intelligent Transportation Systems*, vol. 15, no. 4, pp. 1527–1537, 2014.